INFLUENCE OF OCTAHEDRAL CATION DISTRIBUTION IN MONTMORILLONITE ON INTERLAYER HYDROGEN COUNTER-ION RETENTION STRENGTH VIA FIRST-PRINCIPLES CALCULATIONS

Yayu W. Li[1]* ⓘ, Cristian P. Schulthess[1], Kevin Co[2], Sanjubala Sahoo[2], and
S. Pamir Alpay[2,3]

[1]Department of Plant Science and Landscape Architecture, University of Connecticut, Storrs, CT 06269-4067, USA
[2]Department of Material Science and Engineering, University of Connecticut, Storrs, CT 06269, USA
[3]Department of Physics, University of Connecticut, Storrs, CT 06269, USA

Abstract—Although multiple types of adsorption sites have long been observed in montmorillonite, a consistent explanation about the chemical structure of these adsorption sites has not yet been established. Identifying the cation interlayer adsorption sites based on the octahedral cation distribution on montmorillonite was investigated in this study by using a Density Functional Theory (DFT) simulation. A clay structural model ($H[Al_6MgFe]Si_{16}O_{40}(OH)_8$) with a similar composition to Wyoming SWy-1 montmorillonite was built, where two octahedral Al were respectively substituted by Fe and Mg, and H^+ was the charge compensating cation. This model had twenty-one different possible configurations as a function of the distribution of octahedral Al, Fe, and Mg cations. The DFT simulations of 15 of these different configurations showed no preference for the formation of any configuration with a specific octahedral Fe-Mg distance. However, the H^+ adsorption energy was separated into three distinct groups based on the number of octahedral jumps from Fe to Mg atoms. The H^+ adsorption energy significantly decreased with increasing number of octahedral jumps from Fe to Mg. Assuming an even probability of occurrence of 21 octahedral structures in montmorillonite, the percentages of these three groups are 43, 43, and 14%, respectively, which are very close to the three major sites on montmorillonite from published cation adsorption data. These DFT simulations offer an entirely new explanation for the location and chemical structure of the three major adsorption sites on montmorillonite, namely, all three sites are in the interlayer, and their adsorption strengths are a function of the number of octahedral jumps from Fe to Mg atoms.

Keywords—DFT Simulation · Hydrogen Adsorption · Isomorphic Substitution · Montmorillonite · Octahedral Cation Distribution

INTRODUCTION

Montmorillonite is prevalent in nature with a high cation adsorption capacity (CEC) (Sawhney 1972; Cornell 1993), and plays a significant role in controlling the fate and availability of soil contaminants and plant nutrients (Schulthess and Huang 1990; Bradbury and Baeyens 1997; Nolin 1997; Tertre et al. 2009; Siroux et al. 2017; Martin et al. 2018; Ohkubo et al. 2018). Montmorillonite is a 2:1 phyllosilicate, with two Si tetrahedral sheets sandwiching one Al octahedral sheet. In montmorillonite, isomorphic substitution occurs mostly in the octahedral sheet, where Al^{3+} cations are substituted by Fe^{3+} or Mg^{2+} cations (Yariv 1992; Sposito 2008). The isomorphic substitution in montmorillonite results in an excess negative charge, which requires interlayer counter cations to maintain the charge balance.

Studying the properties of adsorption sites in montmorillonite is essential for understanding its adsorption mechanisms. Based on the physical structure of montmorillonite, three types of adsorption sites are normally considered: basal surface, interlayer, and edge sites (Sawhney 1972; Cornell 1993). The interlayer sites account for the majority of adsorption capacity on montmorillonite (Schulthess and Huang 1990; Tournassat

et al. 2003; Macht et al. 2011). The cations can be adsorbed strongly on interlayer sites because of the Nanopore Inner-Sphere Enhancement effect (NISE; Ferreira et al. 2011; Schulthess et al. 2011), which states that a cation with low hydration energy can be partially or fully dehydrated inside a nanopore when the size of the nanopore is smaller than the hydrated ionic diameter. Montmorillonite is expansive, and its interlayer space ranges from 0 to 1 nm depending on the water content and interlayer cations present, which is in the same size range as most dehydrated and hydrated cations (Norrish 1954). Molecular simulations showed that Na^+ with higher hydration energy tends to be hydrated in the interlayer space, and K^+ and Cs^+ with lower hydration energy tend to be dehydrated and be strongly adsorbed on the clay interlayer surface (Teppen and Miller 2006; Rotenberg et al. 2009).

The number and type of adsorption sites have been identified by ion-exchange modeling on: illite (Poinssot et al. 1999), smectites (Siroux et al. 2017; Martin et al. 2018), beidellites (Robin et al. 2015, 2017), argillite and clayey sediments (Motellier et al. 2003; Jacquier et al. 2004; Tertre et al. 2009). The H^+ cation is present in all these ion-exchange models as a competing cation. The aqueous H^+ cation has fast

---

mobility (Agmon 1999) and exists in all water solutions, and is thus an inevitable competitor in ion-exchange reactions. Accordingly, ion-exchange models must include H^+ as competitive cations (Poinssot et al. 1999; Motellier et al. 2003; Jacquier et al. 2004; Tertre et al. 2009; Robin et al. 2015, 2017; Siroux et al. 2017; Martin et al. 2018). Fourier-transform infrared (FTIR) spectroscopy and DFT simulations also showed that hydronium cations are likely to be intercalated in the interlayer space of hydrated illite and exchange with K^+ cations (Escamilla-Roa et al. 2016). Therefore, the adsorption of counter cations on montmorillonite is evaluated normally with ion adsorption envelopes using the H^+ cation as a competing reference (Schulthess and Huang 1990; Nolin 1997; Bradbury and Baeyens 1997; Tertre et al. 2009; Siroux et al. 2017). The cations adsorbed at low pH have strong adsorption strength, while cations adsorbed at higher pH have weaker adsorption strength. The saturation of each type of adsorption site is extrapolated from the various plateaus in the cation adsorption envelope curves.

Accordingly, in a study of heavy-metal adsorption on Wyoming SWy-1 montmorillonite, Schulthess and Huang (1990) grouped the adsorption sites into three types, involving two edge sites (Si-related sites and Al-related sites) and one strong interlayer site, based on three plateaus observed in their adsorption envelope curve. Similarly, three types of adsorption sites were proposed for Na^+ adsorption on a Wyoming SWy-1 montmorillonite by Nolin (1997), which was based on observance of three plateaus in their Na^+ adsorption envelope curve. Other studies involving adsorption isotherm and adsorption envelope modeling of very low cation concentrations have proposed that a fourth site with high cation adsorption affinity but low capacity (<1% of CEC) might exist on montmorillonite (Bradbury and Baeyens 1997; Tertre et al. 2009; Martin et al. 2018). Thus, three major sites account for the majority of the CEC on montmorillonite (Schulthess and Huang 1990; Bradbury and Baeyens 1997; Nolin 1997; Tertre et al. 2009; Siroux et al. 2017; Martin et al. 2018). Although the nature and location of the proposed three major adsorption sites on montmorillonite still remains speculative, the general opinion is that each site corresponds to a unique surface metal (e.g. aluminol or silanol sites) (Schulthess and Huang 1990) and/or structural location (e.g. edge or interlayer sites) (Bradbury and Baeyens 1997; Martin et al. 2018).

Cation adsorption in the interlayer space is influenced by the charge distribution in the clay. A Grand Canonical Monte Carlo simulation showed that adsorbed Na^+ cations tend to be located in the vicinity of isomorphic substitutions on clay minerals, where the negative charge is more concentrated (Chatterjee et al. 1999). A DFT simulation showed that alkali cations tend to be adsorbed on interlayer sites that are near the tetrahedral Al/Si substitution on dry montmorillonite (Shi et al. 2013). The negative charge distribution, geometry, and surface properties in the vicinity of isomorphic substitutions in clay minerals are influenced by their local environments, such as tetrahedral or octahedral cation distribution and species of neighboring cations (Yariv 1992; Lavikainen et al. 2015; Ohkubo et al. 2018).

Various studies have shown that octahedral cation distribution is very diverse due to the different cation species present, the amount of different cations present, and the spatial distribution of these cations (Muller et al. 1997; Sainz-Diaz et al. 2001; Vantelon et al. 2003; Finck et al. 2015). The analysis of powder diffraction, extended X-ray absorption fine structure (EXAFS) spectroscopy, and vibration infrared (IR) spectroscopy in combination with the chemical composition showed that multiple types of octahedral Al, Mg, Fe cation distribution exist in montmorillonite from Camp-Bertaux, and Fe and Mg tend to segregate in small clusters (Muller et al. 1997). After analyzing 20 illite-smectite interstratified clay samples using FTIR, Al magic angle spinning nuclear magnetic resonance (MAS-NMR) spectroscopy, and Monte Carlo simulations, an increase in illite content showed an increase in octahedral Fe segregation, as well as an increase in the dispersal of octahedral Mg (Cuadros et al. 1999). Using IR and EXAFS spectroscopy, Vantelon et al. (2003) grouped montmorillonite clays into three types according to the number of Fe-Fe pairs in the octahedral sheet: (1) samples from Wyoming (0.45–0.47 Fe per formula unit) showed an ordered distribution of Fe cations, (2) samples from China, Georgia, Milos, and Washington (0.1–2.7 Fe per formula unit) presented a nearly random distribution of Fe cations, and (3) samples from Texas, Bavaria, North Africa, and Arizona (0.14–0.57 Fe per formula unit) exhibited a strong tendency for Fe clustering. A polarized EXAFS study on the structural Fe in Wyoming montmorillonite showed a random distribution of the octahedral Fe (Finck et al. 2015). Also, montmorillonites from different sources but with similar chemical composition can have very different octahedral cation distributions (Tsipursky and Drits 1984; Drits et al. 2006).

Montmorillonite is a dioctahedral clay mineral with a vacancy in every third octahedron. Based on the position of the octahedral hydroxyls, both *cis*-vacant (*cv*) and *trans*-vacant (*tv*) configurations occur in the clay minerals (Drits et al. 2006). The *cv* has two octahedral hydroxyls located on the same side of a vacancy. The *tv* has two octahedral hydroxyls located on opposite sides of a vacancy. Using oblique-texture electron diffraction analysis, a wide percentage of *cv* and *tv* structures has been found in 30 dioctahedral smectites of different composition and genesis (Tsipursky and Drits 1984). After reviewing 26 dioctahedral 2:1 phyllosilicates, Drits et al. (2006) summarized three types of smectites: (1) *cv*, (2) *tv*, or (3) interstratified layers with *cv* or *tv* sheets. The structural iron content in smectites was suggested to be the main factor governing the formation of *cv* and *tv* layers, with high-iron content (>0.6 Fe per formula unit) resulting in dominant *tv* structures, while low-iron content (<0.6 Fe per formula unit) were forming *cv* structures (Wolters et al. 2009; Neumann et al. 2011).

The formation of each type of structure is influenced by the layer composition and the local ordered-disordered distribution of octahedral cations (Drits et al. 2006; Wolters et al. 2009). The local structure, in turn, will influence the geometry of the clay structure and electronic distribution (Yariv 1992; Chatterjee et al. 1999; Sainz-Diaz et al. 2001; Hernández-Haro et al. 2014). After an extensive literature review,

Benson ([1982](#)) tabulated ion-exchange data of clay minerals, and suggested that the variations in crystal chemistry (e.g. chemical composition and structural cation distribution) in smectites were the main factor causing the variability of ion-exchange data.

The octahedral cation distribution, *cv/tv* structure, and cation adsorption sites are difficult to identify due to the small crystal size of clay minerals (Sainz-Diaz et al. [2001](#); Ortega-Castro et al. [2010](#)), variable cation distributions in the clay structure (Cuadros et al. [1999](#); Lavikainen et al. [2015](#)), and clay layer stacking (Drits et al. [2006](#); Ortega-Castro et al. [2010](#); Finck et al. [2015](#)). First-principles DFT simulations have been a potent tool in the calculations of the stable geometry of clay minerals and cation adsorption properties. For example, Ortega-Castro et al. ([2010](#)) simulated the crystallographic properties of dioctahedral 2:1 phyllosilicate using DFT calculations, and demonstrated that tetrahedral Al^{3+} ions are highly dispersed and the interlayer cations are likely to be in the same ditrigonal cavity as the tetrahedral Al^{3+} substitution, where the negative charge is more concentrated. Kaufhold et al. ([2017](#)) investigated the correlations between iron content, fraction of tetrahedral charge, and ratio of *tv* to *cv* structures on dioctahedral smectites using DFT simulations, and found that the energy difference of the clay lattice with different chemical compositions were comparably small, which may result in structural variations of natural clay minerals.

Understanding the influence of the octahedral cation distribution on the clay's cation adsorption strength should help to identify the nature and properties of adsorption sites in clay minerals. The physical and chemical properties in the vicinity of isomorphic substitution should affect the clay's cation adsorption strength. The aim of the present study was to investigate the impact of various octahedral cation distributions on the retention strength of counter cations on montmorillonite using DFT simulations, where H^+ was chosen as the competing reference cation in the simulations.

MATERIALS AND METHODS

A dry H-montmorillonite structure of $(H_{0.5})[Al_3Mg_{0.5}Fe_{0.5}]Si_8O_{20}(OH)_4$ was used, which is similar to the hydrogen form of natural SWy-1 (SWy-2 or SWy-3) montmorillonite: $(Ca_{0.12}Na_{0.32}K_{0.05})[Al_{3.01}Fe_{0.41}Mn_{0.01}Mg_{0.54}Ti_{0.02}]Si_{7.98}Al_{0.02}O_{20}(OH)_4$ (The Clay Minerals Society [2019](#)). Octahedral Fe distribution in SWy-1 (SWy-2 or SWy-3) montmorillonite is believed to be ordered (Vantelon et al. [2003](#); Finck et al. [2015](#)). Accordingly, several ordered configurations of octahedral cation distributions were investigated. The proposed unit formula was $H[Al_6MgFe]Si_{16}O_{40}(OH)_8$, where two octahedral Al cations are substituted by Fe and Mg cations.

The *cv* and *tv* structures and the relative position of octahedral Fe to Mg yielded a total of 21 different possible configurations (Table [1](#)). For the *cv* structures, the octahedral OHs can be placed on the same side or on the opposite side of the octahedral Mg cation, which correspond to *cis*-Mg or *trans*-Mg structures, respectively. For *tv* structures, the OHs can be

placed only at the same side of the octahedral Mg cation, and form only *cis*-Mg structures. Accordingly, there are a total of three groups of structures: *cis*-vacant *cis*-Mg, *cis*-vacant *trans*-Mg, and *trans*-vacant *cis*-Mg. For each group of structures, Fe can be placed next to Mg (noted by *j* = 1), or further away (noted by *j* = 2 or 3), where *j* refers to the number of octahedral jumps from Fe to Mg. Using the Mg octahedron as the reference, Fe can be placed in one of three ways at *j* = 1 and 2, but only one way for a separation of *j* = 3. Enantiomers also exist for each of these, but their electronic properties and structural energies should be identical to their mirror images.

Initial geometries were taken from models proposed by Viani et al. ([2002](#)). The structure is orthorhombic with lattice constants $a = 10.36$ Å, $b = 8.97$ Å, $c = 9.5$ Å, and with a 2.86 Å interlayer space. The initial location of the charge compensating H^+ was put in the ditrigonal cavities. Lattice vectors and the atomic positions of the doped models were thoroughly optimized to eliminate residual interatomic forces.

Computational Methods

For all configurations, the extra H^+ was always bound to the oxygen atom of Mg-OH. The models that span the three possible Fe-Mg distances were selected because the Mg-Fe distance was expected to represent the most significant difference among all configurations. Two permutations per row for rows with *j* = 1 or 2 were selected from a symmetry point of view, as noted by asterisks in Table [1](#). The down selection of fifteen configurations was expected to be sufficient to represent the possible separation distances.

Crystal models were generated by substituting Mg and Fe for Al in the octahedral sheet of pure pyrophyllite. The Mg substitution caused a charged defect, and the added H^+ cation was found to bind to Mg-OH, resulting in the H^+ bond resting normal to the ditrigonal cavity (Sposito [2008](#)).

Super cell calculations were performed using the spin-polarized density functional theory within the generalized gradient approximation (GGA) where the Perdew-Burke-Ernzerhof (PBE) parametrization was used (Perdew et al. [1996](#)). The core and valence electrons were treated with the projector augmented wave method (Blöchl [1994](#)) and the kinetic energy cutoff for the plane waves was set to 500 eV. The supercell for the basic model without adsorbed H^+ consisted of 80 atoms. The energy cut-off for the plane wave basis set was chosen as 500 eV, which was 25% larger than the highest value of cut-off energy in the pseudopotentials of the atomic species. The integrations in the Brillouin zone were performed in a discretized Monkhorst-Pack *k*-points mesh of 5×5×5. Consideration of crystal symmetry reduced the number of independent *k*-points to 63 (Monkhorst and Pack [1976](#)). Geometrical optimization for the models was carried out using the conjugate gradient method where the tolerance for total energy convergence was set to 10^{-6} eV. This amount of energy tolerance ensured a force tolerance of 0.001 eV/Å. The Vienna *ab initio* simulation package (VASP) was used for all computations using the plane wave basis sets (Kresse and Furthmüller [1996](#); Kresse and Joubert [1999](#); Gajdoš et al. [2006](#)).

Table 1. The 21 different octahedral configurations in montmorillonite. F: octahedral Fe; M: octahedral Mg; *cis*-Mg: octahedral OHs are on the same Mg-octahedral edge; *trans*-Mg: octahedral OHs are on the opposite points of the Mg-octahedra; H2: indicates the location of the hydrogen counter cation. Asterisks (*) denote structures used in the DFT simulations

	Fe-Mg Octahedral Jumps, *j*	Configurations		
***cis*-vacant *cis*-Mg**	3	(A)*		
	2	(B)*	(C)*	(D)
	1	(E)*	(F)*	(G)
***cis*-vacant *trans*-Mg**	3	(H)*		
	2	(I)*	(J)*	(K)
	1	(L)*	(M)*	(N)
***trans*-vacant *cis*-Mg**	3	(O)*		
	2	(P)	(Q)*	(R)*
	1	(S)*	(T)	(U)*

H⁺ Adsorption Energy Analysis

   The H⁺ adsorption energy (HAE) was calculated as follows:

$$\text{HAE} = E_{w/H} - \left(E_{w/o\ H} + \mu_H \right) \qquad (1)$$

where $E_{w/H}$ is the total energy of the system with H⁺ cation adsorbed for charge compensation, $E_{w/o\ H}$ is the total energy of the same structure without the H⁺, and μ_H is the chemical potential of the H⁺ cation. The μ_H was

calculated based on two different types of H^+: the H^+ in the H_2O molecule (H-poor), and H^+ in its pure atmospheric form (H-rich). The μ_H in the H-poor condition was calculated with equation (2), and the μ_H in the H-rich condition was calculated with DFT simulations via equation (3):

$$\mu_H(poor) = \frac{1}{2}\left(E_{H_2O} - E_{O_2}/2\right) \qquad (2)$$

$$\mu_H(rich) = E_{H_2}/2 \qquad (3)$$

where E_{H_2O}, E_{O_2}, and E_{H_2} are the total potential energy of H_2O, O_2, and H_2 molecules, respectively. The values of E_{H_2O} (–15.58 eV) and E_{O_2} (–9.85 eV) were obtained from the database Materials Project https://materialsproject.org/, and were kept fixed to calculate the HAE for all cases. The value of E_{H_2} (–6.69 eV) was calculated from the optimized total energy of the H_2 molecule. Statistical analysis of variance of the geometrical parameters, total potential energies, and HAE values were performed using RStudio software (Version 1.2.5019; RStudio 2019).

RESULTS AND DISCUSSION

Optimized Geometry and Total Potential Energy of Different Configurations

Atomic and bond details of the resultant 15 montmorillonite structural models from this DFT study are shown in the Supplementary Materials section. Configuration A with alternate locations for Fe atoms is shown as an example of an optimized structure in Fig. 1. Slight variations were noted in the clay structures with different octahedral cation distributions (Table 2). The a dimension of cv configurations (10.47 ± 0.02 Å) were smaller ($p < 0.001$) than the tv ones (10.54 ± 0.01 Å). The b dimension of cv configurations (9.10 ± 0.01 Å) were larger ($p < 0.001$) than the tv ones (9.06 ± 0.02 Å), but the c dimension (9.57 ± 0.06 Å) was not significantly different for all configurations. The α angles of cis-Mg configurations (90.08 ± 0.14°) were larger ($p < 0.001$) than the $trans$-Mg ones (89.49 ± 0.05°). The β (91.01 ± 0.26°) and γ (89.98 ± 0.10°) angles showed no significant differences among the configurations. The slight variations observed were due to the different ionic radii of the octahedral cations in each clay structure: Al^{3+} (0.61 Å), Mg^{2+} (0.80 Å,) and Fe^{3+} (0.73 Å). Similar results were also obtained in DFT simulations of smectites where the a, c, and β parameters of cv structures were smaller than tv ones (Sainz-Diaz et al. 2001).

These structural and elemental variations resulted in internal energy stresses expressed by the total potential energy of the clay (Table 3). The average of all the total potential energies of the structures with and without charge-compensating H^+ were –587.90 eV and –583.62 eV, respectively. The changes of total potential energy were within 0.42 eV and 0.52 eV for configurations with ($E_{w/H}$) and without ($E_{w/o\ H}$) charge-compensating H^+. These values were within 0.07% and

0.09% of the average total potential energy of structures with and without charge-compensating H^+, respectively. These energy differences of different configurations were very small considering the size of the supercell structure studied (80 or 81 atoms). These small energy differences came from the interactions among Al^{3+}, Mg^{2+}, and Fe^{3+} cations as first, second, and third neighbors in the octahedral sheet. Small energy differences of simulated clay structures with different dioctahedral cation distributions were also observed in other DFT studies (Sainz-Diaz et al. 2001; Hernández-Laguna et al. 2006; Tunega et al. 2007; Ortega-Castro et al. 2010; Hernández-Haro et al. 2014; Ohkubo et al. 2018).

The relative energy was obtained by setting the minimum energy of structure R as 0 eV. The average of the relative energy change ($\Delta E_{w/H}$) of cis-vacant cis-Mg structures (0.34 ± 0.05 eV) revealed no significant difference from the cis-vacant $trans$-Mg structures (0.30 ± 0.07 eV), but both were significantly larger ($p < 0.001$) than the $trans$-vacant cis-Mg structures (0.13 ± 0.08 eV) (Fig. 2). Therefore, the tv configurations were more stable than the cv ones, and the relative position of octahedral hydroxyls (cis-Mg vs $trans$-Mg) did not influence the stability of the structures. Using DFT simulations, Tunega et al. (2007) also showed that the tv structures were more stable than the cv structures when isomorphic substitution occurred in the octahedral sheet.

Additionally, these small energy differences suggest that cv and tv structures can be transformed from one to the other, which is substantiated in the literature. Dehydroxylation-rehydroxylation reactions of two dioctahedral micas (celadonite and glauconite) resulted in the transformation of the tv structure into the cv structure (Muller et al. 2000). Similarly, a cv montmorillonite was transformed into a tv structure by dehydroxylation at high temperature (510–630°C) and subsequent rehydroxylation under steam between 1.5 and 8.0 MPa (Emmerich and Kahr 2001). Using hydrothermal treatments, the proportion of cv and tv layers in synthesized low-charge beidellites can be modified by controlling the synthesis pressure, temperature, and starting materials (Lantenois et al. 2008). This also suggests that the probability of occurrence of natural smectites with similar composition and structure should be nearly equal.

The octahedral Fe-Mg distance did not significantly influence the stability of the various configurations, where the relative total potential energies were 0.21 ± 0.12, 0.26 ± 0.15, and 0.29 ± 0.08 eV for j = 3, 2, and 1, respectively (Table 3, Fig. 2). Therefore, no significant preference should occur for the formation of any specific structure with a specific octahedral Fe-Mg distance. That is, the octahedral Al, Fe, and Mg atoms in this mineral should be randomly distributed. Accordingly, the relative possibilities of the formation of configurations with j = 3, 2, and 1 were 1/7, 3/7, and 3/7, respectively, regardless of the presence of cv or tv, and cis- or $trans$-Mg structures.

Influence of Fe Octahedra on the H^+ Adsorption Strength

The H^+ adsorption energies (HAE) were calculated for two H^+ environments: H-rich and H-poor conditions (Table 3). The
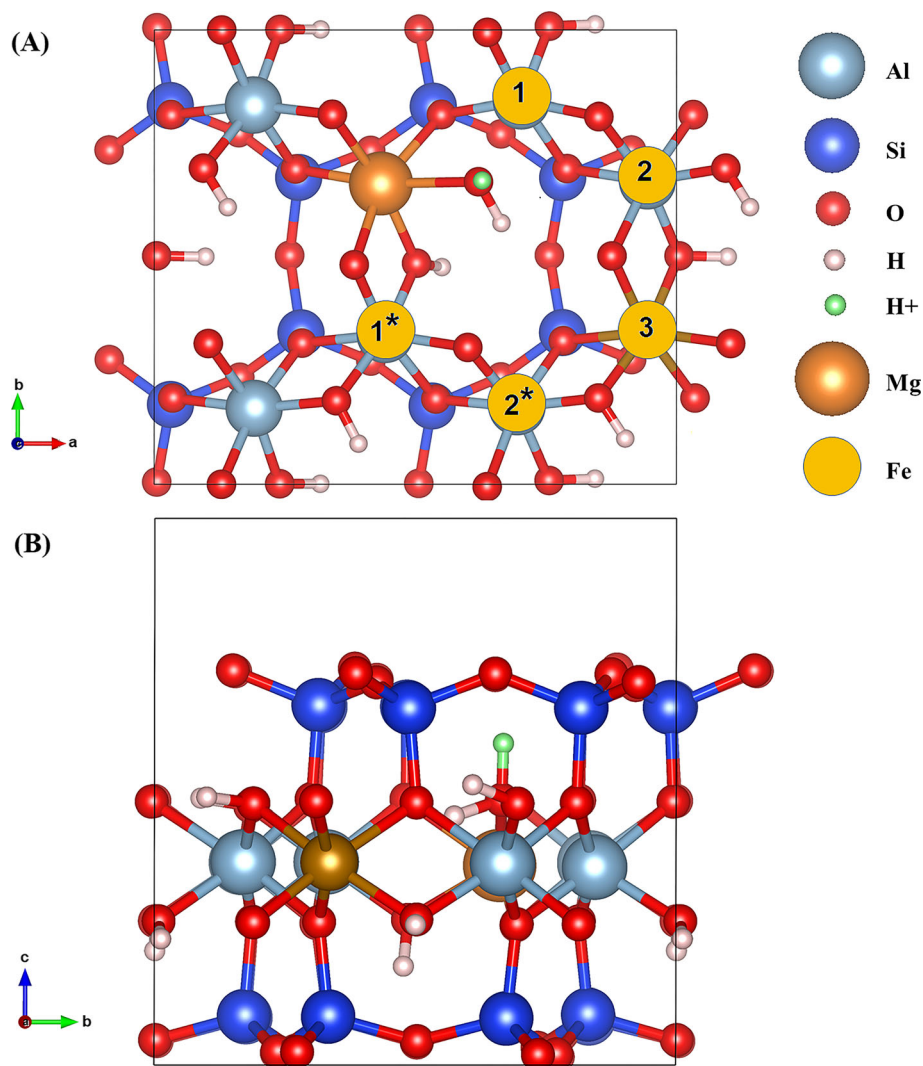
Fig. 1. A [001] (**A**) and [100] (**B**) projection of *cis*-vacant *cis*-Mg montmorillonite supercell model with the top plane of silica removed for clarity for the [001] projection. The positions of Mg and H$^+$ are kept fixed in all models; Fe replaces Al in the octahedral sheet and is indexed by the number of octahedral jumps (j) separating Fe from Mg. The digits (1 to 3, 1* and 2*) indicate the several octahedral jumps of Fe positioned with respect to the Mg within the clay structure.

HAE of configurations in the H-poor environment were 1.98 eV higher than the HAE values in the H-rich environment because of the difference in the μ_H value for H-rich versus H-poor environments. The negative values of HAE in the H-rich environment indicated that the H$^+$ adsorption was an exothermic reaction, and the clay preferred to adsorb the added H$^+$. The positive HAE values in the H-poor environment indicated that the H$^+$ adsorption was an endothermic reaction and the H$^+$ adsorption strength was very weak. The more negative HAE values corresponded to higher H$^+$ adsorption stability.

A strong linear correlation of HAE with the direct Fe-Mg distance was found for both H-rich and H-poor environments ($R^2 = 0.83$, Fig. 3). The results were separated into three distinct groups (labeled 1, 2, and 3) based on the number of octahedral jumps (j) from Fe to Mg and HAE values. The average HAE values were -0.78 ± 0.05, -0.99 ± 0.05,

and -1.12 ± 0.03 eV for groups 1, 2, and 3 in the H-rich environment, respectively. These average HAE values were significantly different from each other ($p < 0.001$). Accordingly, the H$^+$ adsorption stability increased significantly as a function of Mg-Fe distance: group 1 < group 2 < group 3.

The influence of the relative distance of octahedral Fe to Mg on the H$^+$ adsorption strength (Fig. 3) can be ascribed to the electronegativity of these cations. The electronegativity of Fe^{3+} (1.83) is larger than Al^{3+} (1.61) and Mg^{2+} (1.31) (Pauling 1960). Thus, the Fe^{3+} cation tends to pull electrons toward itself and influences the polarity of bonds within these ions. The closer the Fe^{3+} cation was to the Mg^{2+} cation, the more electrons were pulled away from Mg^{2+}, causing diffusion of the electron charge density of the Mg^{2+} cation and a weaker adsorption strength of the H$^+$ cation. Similarly, Lavikainen

Table 2. The optimized main lattice parameters (length in Ångstroms and angles in degrees)

Configurations	a	b	c	α	β	γ
(A)	10.44	9.08	9.53	89.9	91.0	90.0
(B)	10.49	9.11	9.54	90.1	90.9	90.0
(C)	10.49	9.11	9.54	90.1	90.9	90.0
(E)	10.49	9.09	9.55	90.0	90.8	90.1
(F)	10.49	9.09	9.55	90.0	90.8	90.1
(H)	10.46	9.08	9.69	89.4	91.3	90.1
(I)	10.48	9.11	9.50	89.5	90.6	89.9
(J)	10.48	9.11	9.50	89.5	90.6	89.9
(L)	10.46	9.10	9.60	89.5	91.0	89.9
(M)	10.46	9.10	9.60	89.5	91.0	89.9
(O)	10.55	9.07	9.66	90.0	91.4	90.1
(Q)	10.55	9.07	9.66	90.0	91.4	90.1
(R)	10.55	9.07	9.66	90.0	91.4	90.1
(S)	10.53	9.04	9.50	90.3	91.2	89.9
(U)	10.53	9.04	9.50	90.3	91.2	89.9

et al. (2015) observed that the distance of Mg-substitutions on montmorillonite affected the electron density around the surface oxygens. An analogous example to this phenomenon was the inductive effect observed in organic compounds, where the distance of the functional group substitutions influences the strength of the bonds (Carey and Sundberg 2007). For example, if X withdraws electrons in X←COO⁻, the anion XCOO⁻ is stabilized and the acid is strengthened (that is, the ratio of XCOO⁻/XCOOH increases). Conversely, if X releases electrons in X→COO⁻, the anion XCOO⁻ is destabilized and the acid is weakened (that is, the ratio of XCOO⁻/XCOOH decreases).

The three groups of configurations with significantly different HAE identified from this DFT simulation were consistent with the observations from published cation adsorption data on Wyoming SWy-1 montmorillonite (Schulthess and Huang 1990; Nolin 1997), which had Mg and Fe concentrations similar to those used in this DFT study. The adsorption capacities of these three types of adsorption sites on Wyoming SWy-1 montmorillonite were 43, 41, and 16% of the total CEC, respectively (Nolin 1997). These values agreed with the relative possibilities of the formation of configurations with $j = 1$, 2, and 3 as noted above, which were 43, 43, and 14%. These ratios will not be influenced by the formation of a certain group of structures. For example, if both *cis-* and *trans-* structures were formed, nine structures out of a total of 21 will be formed with $j = 1$, and the possibility is 43% (0.43 = 9/21). If only the *cv* was present, this resulted in 6 out of 14 structures or 43% (= 6/14). If only the *tv* was present, this resulted in 3 out of 7 structures or 43% (= 3/7). Other combinations will also lead to the same answer, such as *cis*-Mg or *trans*-Mg structures. Similarly, $j = 2$ has 43% probability (= 3/7), and $j = 3$ has 14% probability (= 1/7). Given the similarity of the chemical composition of Wyoming SWy-1 (SWy-2 or SWy-3) montmorillonite with the composition used in these DFT simulations, these percentages should also apply to the natural SWy montmorillonite. This DFT study offered an entirely new

Table 3 The optimized total potential energy of configurations with ($E_{w/H}$) and without ($E_{w/o\ H}$) the charge-compensating H⁺. The relative total potential energy ($\Delta E_{w/H}$) of configurations with H⁺ cations was calculated by using the minimum energy of configuration R as 0 eV. The HAE indicate the H⁺ adsorption energy in H-rich or H-poor environments for each configuration. Configurations correspond to those shown in Table 1.

| Configurations	$E_{w/H}$ (eV)	$\Delta E_{w/H}$ (eV)	$E_{w/o\ H}$ (eV)	HAE (eV) H-rich	H-poor
(A)	-587.84	0.32	-583.34	-1.16	0.83
(B)	-587.79	0.37	-583.45	-0.99	0.99
(C)	-587.75	0.41	-583.49	-0.91	1.07
(E)	-587.9	0.26	-583.79	-0.77	1.22
(F)	-587.82	0.34	-583.67	-0.81	1.18
(H)	-587.94	0.22	-583.47	-1.13	0.86
(I)	-587.84	0.32	-583.49	-1.01	0.98
(J)	-587.88	0.28	-583.48	-1.05	0.93
(L)	-587.88	0.28	-583.82	-0.72	1.27
(M)	-587.74	0.42	-583.51	-0.88	1.1
(O)	-588.07	0.09	-583.64	-1.09	0.9
(Q)	-588.01	0.15	-583.73	-0.93	1.05
(R)	-588.16	0	-583.77	-1.04	0.94
(S)	-587.94	0.22	-583.86	-0.74	1.25
(U)	-587.97	0.19	-583.84	-0.78	1.2
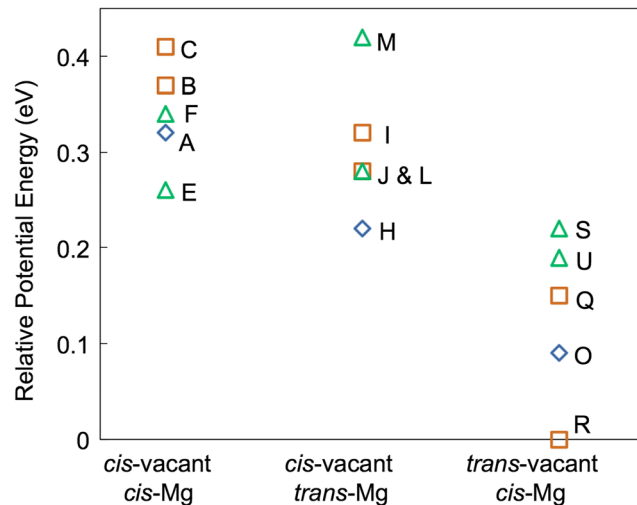
Fig. 2. The optimized total relative potential energy $\Delta E_{w/H}$ with the charge-compensating H^+ for each configuration. Configurations correspond to those shown in Table 1. The ▲, ■, and ♦ symbols represent configurations with octahedral jumps from Fe to Mg as 1, 2, and 3, respectively.

explanation of the location and proportion of these three adsorption sites, namely that all three sites could reside in the interlayer, and that the strength of these adsorption sites is a function of the direct octahedral Fe to Mg distance (or number of octahedral jumps between them).

Naturally, external edge and planar sites also exist, but their contributions to the ion-exchange reactions are small relative to the interlayer sites (Schulthess & Huang 1990; McKinley et al. 1995; Bradbury and Baeyens 1997; Missana et al. 2014). Furthermore, if the NISE effect (Ferreira et al. 2011; Schulthess et al. 2011) can be applied to clay minerals, then the strength of adsorption sites in constrained environments (i.e. interlayer sites) can be much stronger than those of non-constrained environments

(i.e. edge and planar sites). This is particularly relevant with weakly adsorbing alkali cations, such as Na^+, that are observed to adsorb surprisingly strongly on montmorillonite at low pH values (pH < 2.5; Nolin 1997). Similarly, Cs^+ cations adsorbed stronger in the constrained interlayer sites of vermiculite than the external (edge and basal) sites (Dzene et al. 2015).

This study can be applied to other 2:1 expansive clay minerals with different isomorphic substitutions. For example, the $Fe^{3+}:Mg^{2+}$ ratio of smectites can vary significantly. Since the electronegativity of Fe^{3+} is greater than Al^{3+}, increasing the number of octahedral Fe^{3+} atoms around the Mg^{2+} atoms should also increase the electronegativity of the environment surrounding the Mg^{2+} atom. Based on the DFT results (Fig. 3), the smectite
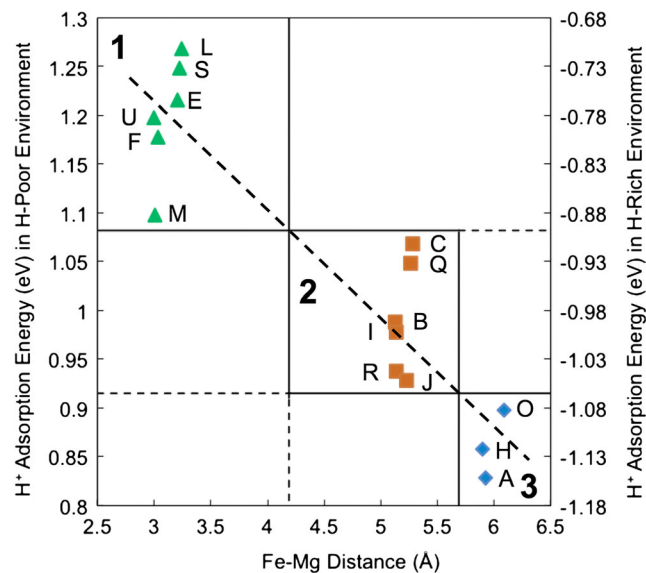

Fig. 3. The H^+ adsorption energy as a function of the Fe-Mg distance under H-rich and H-poor conditions. The letters beside each symbol correspond to the configurations in Table 1. Three groups (labeled 1, 2, and 3) correspond to the number of octahedral jumps from Fe to Mg (noted by j values in Table 1). The dashed line is the linear regression line with $R^2 = 0.83$.

clays with higher $Fe^{3+}:Mg^{2+}$ ratios are presumed to have a weaker affinity toward the H^+ counter cations. The presence of trace levels of other metal substitutions in montmorillonite's octahedral sheet (e.g. Ti^{4+} or Mn^{2+}) could also account for additional adsorption sites, albeit very small. For example, trace levels of a strong fourth site have been proposed in order to improve adsorption model fit, but the location and chemical structure of this fourth site was not specified (Tertre et al. 2009; Martin et al. 2018). Macroscopic data would have trouble distinguishing trace levels of adsorption on trace levels of octahedral substitutions, but statistical correlations of the amount of isomorphic substitution could help resolve this problem. Furthermore, rather than optimizing adsorption site densities and adsorption strengths based only on modeling adsorption data, the adsorption site densities calculated from the chemical structures of the clay minerals would help to simplify and verify the adsorption modeling of clay minerals.

CONCLUSION

Twenty-one configurations of montmorillonite exist when two octahedral Al out of every eight are substituted by Fe and Mg. The DFT simulation showed no preference for the formation of a specific montmorillonite structure. Three groups of configurations with significantly different H^+ adsorption strengths were found as a function of the octahedral Fe to Mg distance. Assuming an even probability of occurrence of 21 octahedral structures in montmorillonite, the percentage of these three groups of configurations were 43, 43, and 14%, which agreed with the three major sites from published experimental adsorption data. This study provided an entirely new explanation of the location and proportion for these three major adsorption sites on montmorillonite. That is, all three major adsorption sites were in the interlayer, and their adsorption strength was a function of the distance of octahedral Fe to Mg. This study confirmed that the adsorption sites on montmorillonite can be influenced by the chemical composition and octahedral cation distribution.

Compliance with Ethical Standards

Conflict of Interest
The authors declare that they have no conflict of interest.

REFERENCES

Agmon, N. (1999). Proton solvation and proton mobility. *Israel Journal of Chemistry, 39*, 493–502.

Benson, L. V. (1982). A tabulation and evaluation of ion exchange data on smectites. *Environmental Geology, 4*, 23–29.

Blöchl, P. E. (1994). Projector augmented-wave method. *Physical review B, 50*, 17953–17979.

Bradbury, M. H., & Baeyens, B. (1997). A mechanistic description of Ni and Zn sorption on Na-montmorillonite. *Part II: Modelling. Journal of Contaminant Hydrology, 27*, 223–248.

Carey, F.A., & Sundberg, R.J. (2007). Advanced organic chemistry. Part A: Structure and mechanisms. Springer Science & Business Media.

Chatterjee, A., Iwasaki, T., Ebina, T., & Miyamoto, A. (1999). A DFT study on clay-cation-water interaction in montmorillonite and beidellite. *Computational Materials Science, 14*, 119–124.

Cornell, R. (1993). Adsorption of cesium on minerals: A review. *Journal of Radioanalytical and Nuclear Chemistry, 171*, 483–500.

Cuadros, J., Sainz-Diaz, C. I., Ramirez, R., & Hernandez-Laguna, A. (1999). Analysis of Fe segregation in the octahedral sheet of bentonitic illite-smectite by means of FTIR, ^{27}Al MAS NMR and reverse Monte Carlo simulations. *American Journal of Science, 299*, 289–308.

Drits, V. A., McCarty, D. K., & Zviagina, B. B. (2006). Crystal-chemical factors responsible for the distribution of octahedral cations over *trans-* and *cis*-sites in dioctahedral 2:1 layer silicates. *Clays and Clay Minerals, 54*, 131–152.

Dzene, L., Tertre, E., Hubert, F., & Ferrage, E. (2015). Nature of the sites involved in the process of cesium desorption from vermiculite. *Journal of Colloid and Interface Science, 455*, 254–260.

Emmerich, K., & Kahr, G. (2001). The *cis-*and *trans*-vacant variety of a montmorillonite: an attempt to create a model smectite. *Applied Clay Science, 20*, 119–127.

Escamilla-Roa, E., Nieto, F., & Sainz-Díaz, C. I. (2016). Stability of the hydronium cation in the structure of illite. *Clays and Clay Minerals, 64*, 413–424.

Ferreira, D. R., Schulthess, C. P., & Giotto, M. V. (2011). An investigation of strong sodium retention mechanisms in nanopore environments using nuclear magnetic resonance spectroscopy. *Environmental Science and Technology, 46*, 300–306.

Finck, N., Schlegel, M. L., & Bauer, A. (2015). Structural iron in dioctahedral and trioctahedral smectites: A polarized XAS study. *Physics and Chemistry of Minerals, 42*, 847–859.

Gajdoš, M., Hummer, K., Kresse, G., Furthmüller, J., & Bechstedt, F. (2006). Linear optical properties in the projector-augmented wave methodology. *Physical Review B, 73*, (045112), 1–9.

Hernández-Laguna, A., Escamilla-Roa, E., Timón, V., Dove, M. T., & Sainz-Díaz, C. I. (2006). DFT study of the cation arrangements in the octahedral and tetrahedral sheets of dioctahedral 2:1 phyllosilicates. *Physics and Chemistry of Minerals, 33*, 655–666.

Hernández-Haro, N., Ortega-Castro, J., Pruneda, M., Sainz-Díaz, C. I., & Hernández-Laguna, A. (2014). Theoretical study on the influence of the Mg^{2+} and Al^{3+} octahedral cations on the vibrational spectra of the hydroxy groups of dioctahedral 2:1 phyllosilicate models. *Journal of Molecular Modeling, 20*, (2402), 1–10.

Jacquier, P., Ly, J., & Beaucaire, C. (2004). The ion-exchange properties of the Tournemire argillite: I. Study of the H, Na, K, Cs, Ca and Mg behaviour. *Applied Clay Science, 26*, 163–170.

Kaufhold, S., Kremleva, A., Krüger, S., Rösch, N., Emmerich, K., & Dohrmann, R. (2017). Crystal-chemical composition of dicotahedral smectites: An energy-based assessment of empirical relations. *ACS Earth and Space Chemistry, 1*, 629–636.

Kresse, G., & Furthmüller, J. (1996). Efficient iterative schemes for *ab initio* total-energy calculations using a plane-wave basis set. *Physical Review B, 54*, 11169–11186.

Kresse, G., & Joubert, D. (1999). From ultrasoft pseudopotentials to the projector augmented-wave method. *Physical Review B, 59*, 1758–1775.

Lantenois, S., Muller, F., Bény, J. M., Mahiaoui, J., & Champallier, R. (2008). Hydrothermal synthesis of beidellites: Characterization and study of the *cis-*and *trans*-vacant character. *Clays and Clay Minerals, 56*, 39–48.

Lavikainen, L. P., Tanskanen, J. T., Schatz, T., Kasa, S., & Pakkanen, T. A. (2015). Montmorillonite interlayer surface chemistry: Effect of

magnesium ion substitution on cation adsorption. *Theoretical Chemistry Accounts, 134*, (51), 1–7.

Macht, F., Eusterhues, K., Pronk, G. J., & Totsche, K. U. (2011). Specific surface area of clay minerals: Comparison between atomic force microscopy measurements and bulk-gas (N_2) and-liquid (EGME) adsorption methods. *Applied Clay Science, 53*, 20–26.

Martin, L. A., Wissocq, A., Benedetti, M. F., & Latrille, C. (2018). Thallium (Tl) sorption onto illite and smectite: Implications for Tl mobility in the environment. *Geochimica et Cosmochimica Acta, 230*, 1–16.

McKinley, J. P., Zachara, J. M., Smith, S. C., & Turner, G. D. (1995). The influence of uranyl hydrolysis and multiple site-binding reactions on adsorption of U(VI) to montmorillonite. *Clays and Clay Minerals, 43*, 586–598.

Missana, T., Benedicto, A., García-Gutiérrez, M., & Alonso, U. (2014). Modeling cesium retention onto Na-, K- and Ca-smectite: Effects of ionic strength, exchange and competing cations on the determination of selectivity coefficients. *Geochimica et Cosmochimica Acta, 128*, 266–277.

Monkhorst, H. J., & Pack, J. D. (1976). Special points for Brillouin-zone integrations. *Physical Review B, 13*, 5188–5192.

Motellier, S., Ly, J., Gorgeon, L., Charles, Y., Hainos, D., Meier, P., & Page, J. (2003). Modelling of the ion-exchange properties and indirect determination of the interstitial water composition of an argillaceous rock. Application to the Callovo-Oxfordian low-water-content formation. *Applied Geochemistry, 18*, 1517–1530.

Muller, F., Besson, G., Manceau, A., & Drits, V. A. (1997). Distribution of isomorphous cations within octahedral sheets in montmorillonite from Camp-Bertaux. *Physics and Chemistry of Minerals, 24*, 159–166.

Muller, F., Drits, V., Plançon, A., & Robert, J. L. (2000). Structural transformation of 2:1 dioctahedral layer silicates during dehydroxylation-rehydroxylation reactions. *Clays and Clay Minerals, 48*, 572–585.

Neumann, A., Petit, S., & Hofstetter, T. B. (2011). Evaluation of redox-active iron sites in smectites using middle and near infrared spectroscopy. *Geochimica et Cosmochimica Acta, 75*, 2336–2355.

Nolin, D. (1997). Rétention de radioéléments à vie longue par des matériaux argileux. Influence d'anions contenus dans les eaux naturelles. Ph.D. Thesis, Universite Pierre Et Marie Curie, Paris 6.

Norrish, K. (1954). The swelling of montmorillonite. *Discussions of the Faraday Society, 18*, 120–134.

Ohkubo, T., Okamoto, T., Kawamura, K., Guégan, R., Deguchi, K., Ohki, S., Shimizu, T., Tachi, Y., & Iwadate, Y. (2018). New insights into the Cs adsorption on montmorillonite clay from ^{133}Cs solid-state NMR and density functional theory calculations. *The Journal of Physical Chemistry A, 122*, 9326–9337.

Ortega-Castro, J., Hernández-Haro, N., Dove, M. T., Hernández-Laguna, A., & Sainz-Díaz, C. I. (2010). Density functional theory and Monte Carlo study of octahedral cation ordering of Al/Fe/Mg cations in dioctahedral 2:1 phyllosilicates. *American Mineralogist, 95*, 209–220.

Pauling, L. (1960). *The Nature of the chemical bond*. Ithaca, NY: Cornell University Press.

Perdew, J. P., Burke, K., & Ernzerhof, M. (1996). Generalized gradient approximation made simple. *Physical Review Letters, 77*, 3865–3868.

Poinssot, C., Baeyens, B., & Bradbury, M. H. (1999). Experimental and modelling studies of caesium sorption on illite. *Geochimica et Cosmochimica Acta, 63*, 3217–3227.

Robin, V., Tertre, E., Beaufort, D., Regnault, O., Sardini, P., & Descostes, M. (2015). Ion exchange reactions of major inorganic cations (H^+, Na^+, Ca^{2+}, Mg^{2+} and K^+) on beidellite: Experimental results and new thermodynamic database. Toward a better prediction of contaminant mobility in natural environments. *Applied Geochemistry, 59*, 74–84.

Robin, V., Tertre, E., Beaucaire, C., Regnault, O., & Descostes, M. (2017). Experimental data and assessment of predictive modeling for radium ion-exchange on beidellite, a swelling clay mineral with a tetrahedral charge. *Applied Geochemistry, 85*, 1–9.

Rotenberg, B., Morel, J. P., Marry, V., Turq, P., & Morel-Desrosiers, N. (2009). On the driving force of cation exchange in clays: Insights from combined microcalorimetry experiments and molecular simulation. *Geochimica et Cosmochimica Acta, 73*, 4034–4044.

Sainz-Diaz, C. I., Hernández-Laguna, A., & Dove, M. T. (2001). Theoretical modelling of *cis*-vacant and *trans*-vacant configurations in the octahedral sheet of illites and smectites. *Physics and Chemistry of Minerals, 28*, 322–331.

Sawhney, B. (1972). Selective sorption and fixation of cations by clay minerals: A review. *Clays and Clay Minerals, 20*, 93–100.

Schulthess, C. P., & Huang, C. P. (1990). Adsorption of heavy metals by silicon and aluminum oxide surfaces on clay minerals. *Soil Science Society of America Journal, 54*, 679–688.

Schulthess, C. P., Taylor, R. W., & Ferreira, D. R. (2011). The nanopore inner sphere enhancement effect on cation adsorption: Sodium and nickel. *Soil Science Society of America Journal, 75*, 378–388.

Siroux, B., Beaucaire, C., Tabarant, M., Benedetti, M. F., & Reiller, P. E. (2017). Adsorption of strontium and caesium onto an Na-MX80 bentonite: Experiments and building of a coherent thermodynamic modelling. *Applied Geochemistry, 87*, 167–175.

Shi, J., Liu, H., Lou, Z., Zhang, Y., Meng, Y., Zeng, Q., & Yang, M. (2013). Effect of interlayer counterions on the structures of dry montmorillonites with Si^{4+}/Al^{3+} substitution. *Computational Materials Science, 69*, 95–99.

Sposito, G. (2008). *The chemistry of soils*. Oxford University Press.

Teppen, B. J., & Miller, D. M. (2006). Hydration energy determines isovalent cation exchange selectivity by clay minerals. *Soil Science Society of America Journal, 70*, 31–40.

Tertre, E., Beaucaire, C., Coreau, N., & Juery, A. (2009). Modelling Zn (II) sorption onto clayey sediments using a multi-site ion-exchange model. *Applied Geochemistry, 24*, 1852–1861.

The Clay Minerals Society (2019). Physical and chemical data of source clays, http://www.clays.org/sourceclays_data.html, viewed 7 June 2019.

Tournassat, C., Neaman, A., Villiéras, F., Bosbach, D., & Charlet, L. (2003). Nanomorphology of montmorillonite particles: Estimation of the clay edge sorption site density by low-pressure gas adsorption and AFM observations. *American Mineralogist, 88*, 1989–1995.

Tsipursky, S. I., & Drits, V. A. (1984). The distribution of octahedral cations in the 2:1 layers of dioctahedral smectites studied by oblique-texture electron diffraction. *Clay Minerals, 19*, 177–193.

Tunega, D., Goodman, B. A., Haberhauer, G., Reichenauer, T. G., Gerzabek, M. H., & Lischka, H. (2007). *Ab initio* calculations of relative stabilities of different structural arrangements in dioctahedral phyllosilicates. *Clays and Clay minerals, 55*, 220–232.

Vantelon, D., Montarges-Pelletier, E., Michot, L. J., Pelletier, M., Thomas, F., & Briois, V. (2003). Iron distribution in the octahedral sheet of dioctahedral smectites. An Fe K-edge X-ray absorption spectroscopy study. *Physics and Chemistry of Minerals, 30*, 44–53.

Viani, A., Gualtieri, A. F., & Artioli, G. (2002). The nature of disorder in montmorillonite by simulation of X-ray powder patterns. *American Mineralogist, 87*, 966–975.

Wolters, F., Lagaly, G., Kahr, G., Nueeshch, R., & Emmerich, K. (2009). A comprehensive characterization of dioctahedral smectites. *Clays and Clay Minerals, 57*, 115–133.

Yariv, S. (1992). The effect of tetrahedral substitution of Si by Al on the surface acidity of the oxygen plane of clay minerals. *International Reviews in Physical Chemistry, 11*, 345–375.